Available online at www.sciencedirect.com
ScienceDirect
Journal of Nuclear Materials 360 (2007) 75–91
journal of nuclear materials
www.elsevier.com/locate/jnucmat

On the (in)adequacy of the Charpy impact test to monitor irradiation effects of ferritic/martensitic steels

R. Chaouadi *

SCK·CEN, Boeretang 200, 2400 Mol, Belgium

Received 26 March 2006; accepted 30 August 2006

Abstract

Irradiation embrittlement studies rely very often on Charpy impact data, in particular the ductile-to-brittle transition temperature (DBTT). However, while the DBTT-shift is equivalent to the increase of the fracture toughness transition temperature of ferritic steels, it is not the case for ferritic/martensitic steels. The aim of this study is to critically assess experimental data obtained on a 9%Cr–ferritic/martensitic steel, Eurofer-97, to better understand the underlying mechanisms involved during the fracture process. More specifically, a dedicated analysis using the load diagram approach allows to unambiguously reveal the actual effects of irradiation on physically rather than empirically based parameters. A comparison is made between a ferritic and ferritic/martensitic steel to better identify the possible similarities and differences. Tensile, Charpy impact and fracture toughness tests data are examined in a global approach to assess the actual rather than apparent irradiation effects. The adequacy or inadequacy of the Charpy impact test to monitor irradiation effects is extensively discussed.

PACS: 61.80.Hg; 61.82.Bg; 62.20.Mk; 81.40.Np; 81.70.Bt

1. Introduction

For historical reasons, the Charpy impact test was used to monitor irradiation effects of reactor pressure vessel ferritic steels, in particular to determine the ductile-to-brittle transition temperature (DBTT). This transition temperature, indexed to a specific energy-level, was found to correlate well with the nil-ductility temperature (NDT) obtained with Pellini drop-weight test which in turn correlates well to the lower bound fracture toughness curve [1–3]. As a consequence, until today, the Charpy impact test is used as a reference test in the reactor pressure vessel community. In particular, most of irradiation effects are evaluated in terms of the change of DBTT, usually measured at a fixed energy level although, in a few cases, this procedure was questioned [4,5]. The Charpy-based DBTT was also questioned by Odette and Lucas [6] for ferritic/martensitic steels. Hence, correlations such as those established for ferritic steels are not available for ferritic/martensitic steels and these are not necessarily applicable to the latter.

* Tel.: +32 14 33 21 90; fax: +32 14 32 15 29.
E-mail address: rchaouad@sckcen.be

0022-3115/$ - see front matter © 2006 Elsevier B.V. All rights reserved.
doi:10.1016/j.jnucmat.2006.08.025

The last decade has seen the generalization of the use of fracture toughness measurements with small size samples associated to the master curve approach. The method was extensively applied to ferritic steels, validated and an ASTM standard was established [7]. In general, the irradiation-induced shift of the fracture toughness transition curve is found in agreement with the shift of the Charpy impact transition curve. However, the correlations that were established and their validation were demonstrated for ferritic steels. It was implicitly admitted that such correlations still hold for ferritic/martensitic steels which indeed present many similarities with ferritic steels.

With the recent fracture toughness results on ferritic/martensitic steels for the fusion technology, it is found that the DBTT-change of such steels does not reflect the actual irradiation embrittlement. In other words, the shift of the fracture toughness transition curve is systematically greater than the shift of the Charpy-based DBTT change [8–10]. It should be noticed that this is not only inherent to the material specificity, namely ferritic versus martensitic, but the neutron dose range of RPV ferritic and fusion martensitic steels are very different, the end-of-life neutron exposure of an RPV (ferritic) steel is one to two orders of magnitude less than for the fusion blanket ferritic/martensitic steel.

Within the SCK·CEN fusion activities, an important effort is carried out for characterizing irradiation effects on the European reference ferritic/martensitic steel, Eurofer-97 [8,11,12]. In Fig. 1, we reproduced the Charpy impact transition curve behavior with increasing neutron dose. Two observations can already be made. First, the shift of the transition curve is quite small in comparison to other materials for the neutron exposure under consideration, in particular with respect to ferritic steels. Second, the shape of the transition curve is sharper in comparison to ferritic steels. As it will be seen later, the shift of the fracture toughness transition curve is significantly higher than the DBTT-shift.

The main objective of this paper is to analyze the reasons of such a behavior. The concept of the load diagram approach will be used to more accurately define the material behavior using physically based parameters. Also, a detailed comparison between martensitic and ferritic steel will be made to better understand their respective behaviors. Finally, the adequacy or inadequacy of using the Charpy impact test to monitor irradiation effects of ferritic/martensitic steels will be critically evaluated to better assess these materials in terms of structural integrity.

2. Material and experimental conditions

High chromium ferritic/martensitic steels have received a lot of attention by the fusion community during the last decade. These steels were originally developed a half century ago for high temperature applications such as boilers, steam generators and turbines [13]. They were evaluated also in neutron environments for application in in-core fission

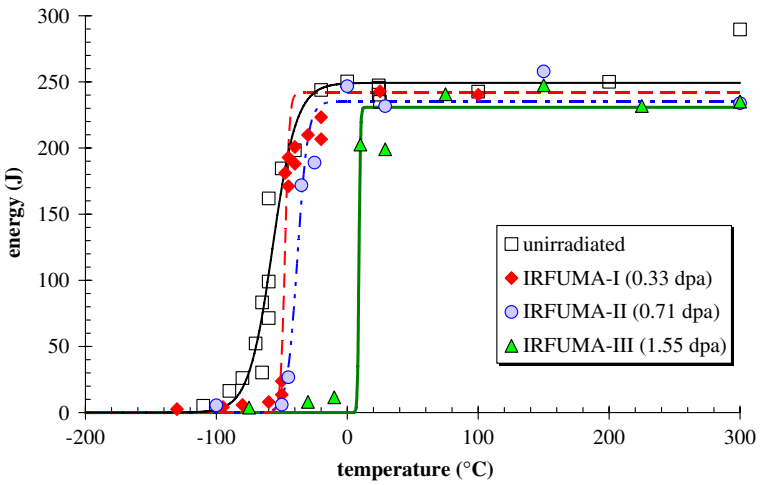

Fig. 1. Charpy impact energy transition behavior of Eurofer-97 for various neutron doses [8,12].

reactor structures such as ducts and cladding. Finally, they were also considered as potential candidates for fusion applications, such as the first wall and breeding blanket structures. The properties of such steels were continuously improved to fit the severe requirements of a number of technological applications. Other requirements related to disposal of radioactive waste led to the development of the so-called reduced- (or low-) activation ferritic/martensitic (RAFM or LAFM) steels by substituting the highly activation elements such as Mo, Nb, Ni by low activation elements W, V, Mn and Ta. One of such a material is Eurofer-97, a 9%Cr–1%W ferritic/martensitic steel. It was developed in Europe and it is extensively investigated within the European fusion research program [8,10–12,14–22]. The microstructure is typically fully martensitic with lath shaped martensite subgrains [16]. The chemical composition and the heat treatment history of this material are given in Table 1.

This material was irradiated at 300 °C for three dose levels at the BR2 reactor. Details on the irradiations conditions can be found elsewhere [8,11,12]. A number of mechanical properties were already reported in [8,12] including tensile, Charpy impact and fracture toughness. Some additional tests, in particular dynamic tensile and fracture toughness tests, were performed to better define the material behavior.

3. Background

In the following, we consider only bcc materials which exhibit a transition from ductile (stable) to brittle (unstable) fracture as a function of temperature. Two terms are usually used to reflect the effects of irradiation on the mechanical properties, namely, hardening and embrittlement. The first one expresses the fact that the nano-size defects induced by irradiation act as obstacles to dislocation motion increasing thereby the yield strength. Hardness and tensile tests are usually used to quantitatively evaluate the irradiation hardening. The second one, embrittlement, expresses the effect of irradiation on the fracture resistance, which is also a consequence of the induced hardening. Indeed, following the Davidenkov diagram, the temperature at which the critical stress for initiating fracture is reached increases with increasing hardening. The irradiation embrittlement is quantified by the increase of this temperature. In practice, Charpy impact tests are used to determine the ductile-to-brittle transition curve from which the transition temperature, DBTT, is derived. The DBTT is usually defined at the midpoint between the upper- and lower-shelf levels. This definition was adopted by the fusion community to evaluate the DBTT. Because of the use of subsized Charpy specimens, an extensive experimental work was done to validate these geometries [23,24].

Considering the experimental data shown in Fig. 1, the DBTT was determined in the unirradiated and the three irradiated conditions. Note that the same trends as in Fig. 1 are observed when the results are plotted in terms of shear fracture appearance or lateral expansion.

Fracture toughness tests were also performed on this material in the unirradiated and the three irradiated conditions. The results are shown in Fig. 2 together with the probability bounds as defined by the master curve procedure. The test temperature is normalized by the reference temperature, $T_{100\,\mathrm{MPa}\sqrt{\mathrm{m}}}$. Although originally developed (and validated) for ferritic steels, the master curve procedure is assumed to be applicable for ferritic/martensitic steels. As it will be seen later, this assumption is believed to be valid if fracture remains typically brittle, without ductile crack extension preceding cleavage. In Fig. 3, we compare the DBTT-shift to the $T_{100\,\mathrm{MPa}\sqrt{\mathrm{m}}}$-shift, indicating clearly the bias introduced by the Charpy impact test for the three neutron exposures. Other transition temperatures based on the shear fracture appearance and lateral expansion lead to a similar bias.

This observation of the underestimation of the transition temperature shift when based on the Charpy impact data is not specific to Eurofer-97 steel, neither to irradiation conditions. Indeed, other materials and irradiation conditions have shown such a behavior. For example, the 12%Cr–1Mo

Table 1
Chemical composition (wt%) and heat treatment of Eurofer-97

Material	C	Ni	Cr	Mo	Cu	Si	Nb	V	P	Mn	W	Ta	Fe
E-97	0.12	0.007	8.99	<0.001	0.022	0.07	<0.001	0.19	<0.005	0.44	1.1	0.14	Bal.

Heat treatments: normalized at 980 °C/1 h 50 min, tempered at 740 °C/3 h 40 min.

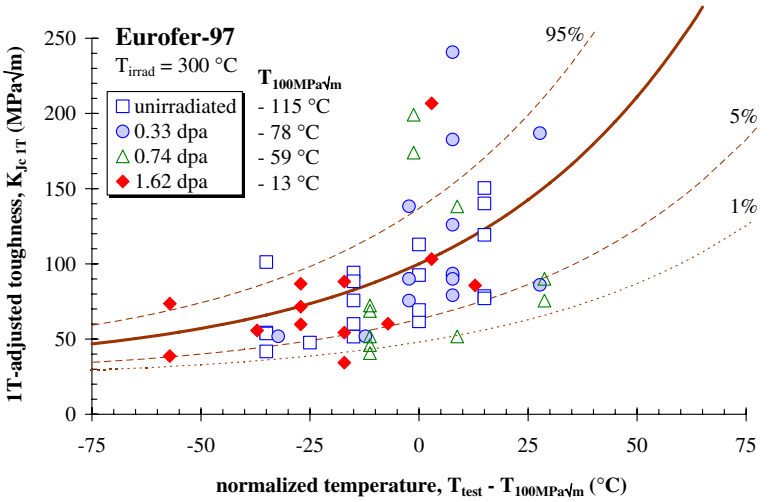

Fig. 2. Fracture toughness in the transition regime of unirradiated and irradiated Eurofer-97.

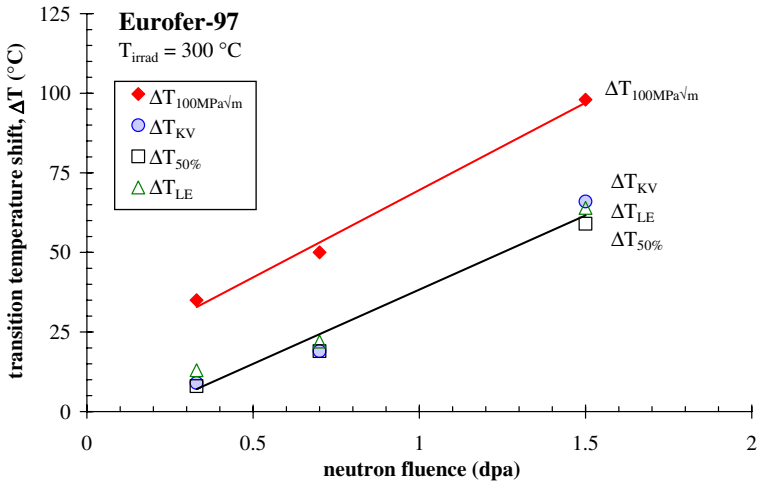

Fig. 3. Significant difference between DBTT-change (ΔT_{KV}, ΔT_{LE}, $\Delta T_{50\%}$) and $T_{100\,MPa\sqrt{m}}$-shift.

ferritic/martensitic steel, HT9, irradiated at 200 °C to a neutron dose of 2.9 dpa exhibited a DBTT-shift measured with KLST-type specimens of 169 °C while the shift of the fracture toughness transition curve, $\Delta T_{100\,MPa\sqrt{m}}$, was found equal to 251 °C [25].

These differences are usually not observed on ferritic steels which normally remain within ±15%-deviation. The question arises whether this is due to the material (ferritic versus martensitic) or to the irradiation conditions (low versus high dpa). In the following, it will be clearly established that these differences are basically inherent to the data analysis procedure and not to the material or irradiation conditions.

In the following, advantage will be taken from the load diagram approach that allows a more fundamental analysis of the Charpy impact data together with the tensile properties.

4. Load diagram approach

The load diagram approach, originally developed by Fabry, is considered as a powerful technique to describe the actual mechanisms of flow and fracture in a Charpy impact test [26–28]. Indeed, instrumented Charpy impact test data allow to construct a diagram in which both flow and fracture properties and the associated fracture surface characteristics are taken into account in a unique way.

Details on the procedure can be found in [26]. As an illustration, Fig. 4 shows the load diagram of Eurofer-97 in the unirradiated condition. The upper part of the diagram is based on the characteristic loads derived from the load–time records and the lower part shows the shear fracture diagram. These two diagrams are uniquely associated.

As a result, the temperature dependence of the flow properties, the microcleavage fracture stress and the crack arrest properties of the material are clearly identified. Thus, a number of characteristic temperatures can be defined, but in contrast to classical DBTT parameters, these temperatures are physically based. For example, the temperature at which fracture occurs at the general yielding, T_I, characterizes the upper temperature at which fracture is fully brittle (SFA = 0%). Another temperature, T_O, can be defined as the temperature above which fracture is fully ductile (SFA = 100%). Another characteristic temperature, T_{NDT}, that was found to be correlated to the nil-ductility temperature, can be defined. Finally, the microcleavage fracture stress can also be derived from such a diagram as it is proportional to the general yield stress at T_I. The load diagram offers a unique description of the flow and fracture properties of a material as a function of test temperature.

The characteristic parameters, determined using the load diagram approach for Eurofer-97 as a function of neutron dose, are given in Table 2. Note that the microcleavage fracture stress does not change with irradiation indicating a similar fracture micromechanism. The relative change of the various transition temperatures are shown in Table 3. Besides

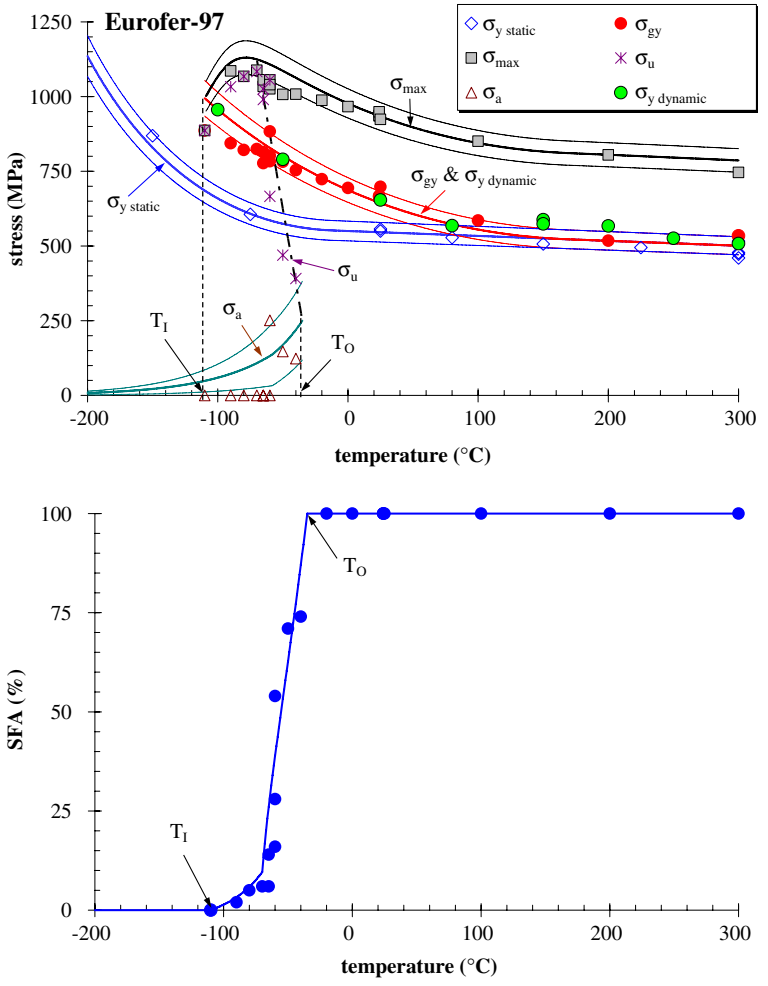

Fig. 4. Load (stress) diagram with its associated SFA diagram of Eurofer-97. At T_I, fracture occurs at general yield. Below T_I, fracture is fully brittle (SFA = 0%). Above T_O, fracture is fully ductile (SFA = 100%).

Table 2
Load diagram parameters of Eurofer irradiated at 300 °C

Dose (dpa)	σ_{ath} (MPa)	σ_c (MPa)	T_I (°C)	T_O (°C)	T_{NDT} (°C)	FATT (°C)	$T_{100\,MPa\sqrt{m}}$ (°C)
0	595	2320	−110	−35	−58	−56	−115
0.33	690	2338	−80	−20	−50	−36	−77
0.71	780	2356	−60	−25	−50	−31	−62
1.55	875	2301	−20	10	−20	5	−14

σ_{ath}: athermal yield strength; σ_c: microcleavage fracture stress; T_I: brittle initiation temperature (when fracture occurs at general yield); T_O: temperature at onset of upper shelf; T_{NDT}: Charpy crack arrest temperature; FATT: transition temperature corresponding to 50%-shear fracture appearance.

Table 3
Temperature shifts of the load diagram parameters

Dose (dpa)	ΔT_I (°C)	ΔT_O (°C)	ΔT_{NDT} (°C)	ΔFATT (°C)	$\Delta T_{100\,MPa\sqrt{m}}$ (°C)
0.33	30	15	8	20	38
0.71	50	10	8	25	53
1.55	90	45	38	61	101

the parameters derived from the load diagram, the fracture toughness transition temperature, $T_{100\,MPa\sqrt{m}}$, is also indicated. As shown in Fig. 5, ΔT_I corresponding to a fully brittle fracture (0% SFA) correlates well with the $\Delta T_{100\,MPa\sqrt{m}}$. This clearly indicates the inadequacy of a DBTT concept based on an arbitrary energy-, SFA- or lateral expansion-level. By contrast, a physically based transition temperature seems to be more adequate. Indeed, the tests on which $T_{100\,MPa\sqrt{m}}$ is determined fail mostly in a fully brittle manner. It is thus not surprising that it correlates well with T_I. Fig. 6 shows such a correlation on a number of ferritic (mainly RPV steels) as well as ferritic/martensitic steels.

5. Ductile-to-brittle transition temperature

The degree of irradiation embrittlement is usually associated with the change of the transition temperature evaluated from Charpy impact tests. This transition temperature is conventionally evaluated at an arbitrary level of absorbed energy, shear fracture appearance or lateral expansion. Most of available transition temperatures are based on an arbitrary level of the absorbed energy [29] although no physical meaning can be associated with such a transition temperature. In the fusion community, these temperatures are commonly evaluated at 50% of the upper shelf plateau or at a level midway between the lower and upper shelves [8–12,30–46]. In some cases, the DBTT is evaluated at a fixed energy level [47–49]. Originally, this definition was chosen by Corwin et al. [50] to validate the use of subsized Charpy with respect to standard Charpy specimens. The same DBTT-definition was used later by Louden et al. [51] to investigate the size and configuration (notch versus crack) of HT9. Later on, this definition was adopted by many

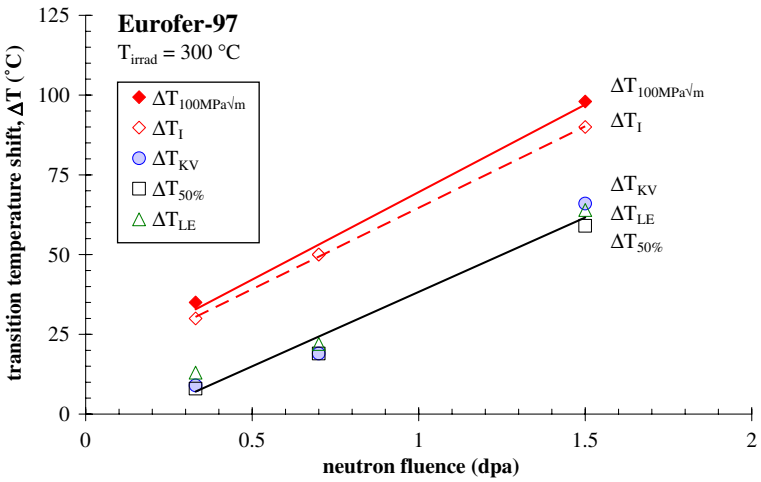

Fig. 5. Comparison of the different transition temperature indexes. Very good agreement is found between $\Delta T_{100\,MPa\sqrt{m}}$ and ΔT_I.

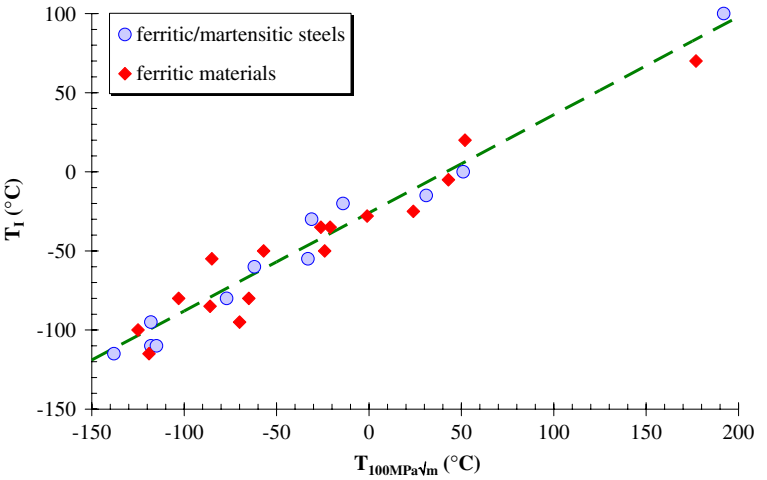

Fig. 6. Correlation between $T_{100\,MPa\,\sqrt{m}}$ and T_I.

investigators for determining the transition temperature. However, the transition curve (shape and position with respect to temperature) varies from one material to another [14,39,40,50,52–55], is affected by the specimen geometry and configuration [51,56] and does not shift in a homologous way [9,33,57–59], and therefore cannot be defined by a unique parameter. This is shown in Fig. 7 which clearly illustrates the shape change of the transition curve with irradiation. Therefore, the DBTT-shift as evaluated at a specific level of energy, shear fracture appearance or lateral expansion will depend on this specific level. On the other hand, the fracture toughness transition curve is uniquely defined by a single transition temperature, arbitrary measured at 100 MPa $\sqrt{m}$ (see Fig. 2). The shape of the Charpy impact transition curve can be modified by irradiation while the fracture toughness transition curve is not. As a result, the shift of the transition curve does not depend on the fracture toughness level at which the transition temperature is determined. This means that depending of the reference level that is chosen to define the Charpy impact transition temperature (DBTT), the correlation between the latter and the fracture toughness transition temperature will be affected. This will be demonstrated later.

It is important to notice that the underestimation of the DBTT-shift using Charpy-V notched specimen with respect to fracture toughness is not due

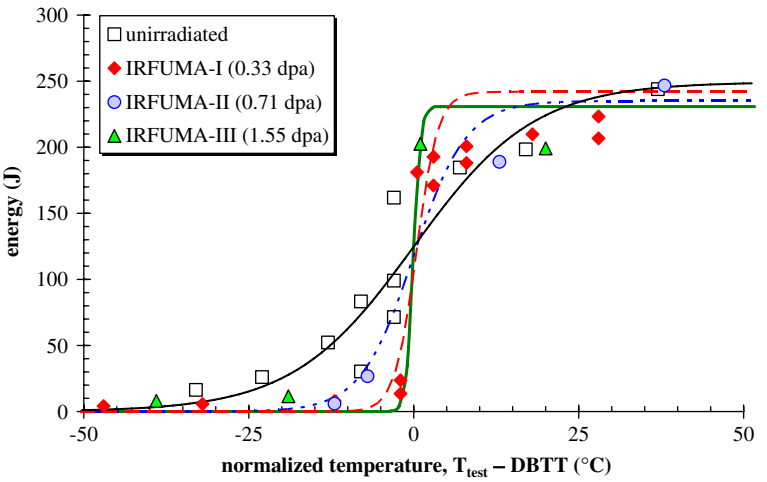

Fig. 7. Change of the transition curve shape with irradiation.

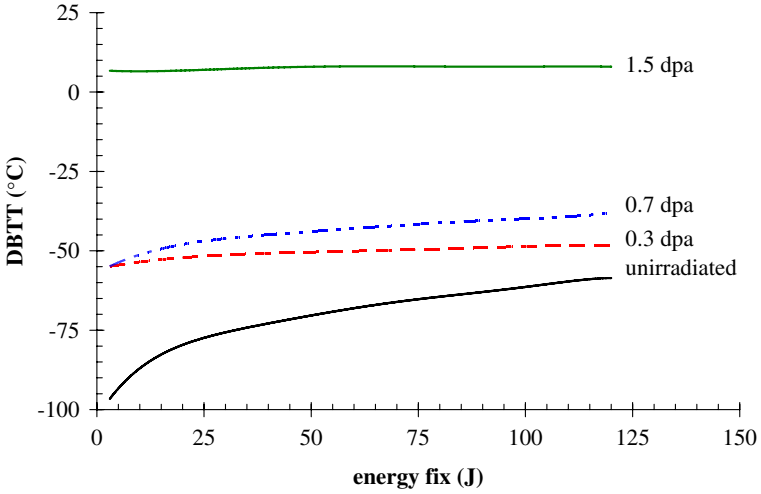

Fig. 8. Variation of the DBTT with the energy fix.

to the effect of notch acuity, as suggested by Rensman et al. [10] but it is inherent to the procedure of DBTT determination. The critical conditions for crack initiation are not altered by the notch. It is also believed that the disagreement between Charpy-V impact and fracture toughness transition shifts is not resulting from loading rate effects. As clearly illustrated by Fig. 7, it is the DBTT definition that plays the key role. Depending on the energy fix that is used to determine the DBTT, the shift with respect to the reference unirradiated state will be different. This is shown in Fig. 8 where the DBTT is plotted as a function of the energy fix. As it can be seen, the DBTT in the unirradiated state varies much with the energy fix and the underestimation of the DBTT-shift observed in the previous section is mainly due to the initial DBTT misevaluation. By decreasing the energy fix, reducing thereby the ductile crack extension contribution, the difference between Charpy impact and fracture toughness transition temperature shifts decreases.

These results emphasize the importance of a well-interpretation of the experimental results and conclusions on irradiation embrittlement resistance drawn from Charpy-based DBTT (standard as well as subsized specimens) should be considered with caution [49].

6. Comparison between ferritic and ferritic/martensitic steels

The deviations between Charpy impact and fracture toughness transition curves were observed on many others martensitic steels [9,25,53,54]. As already mentioned, the use of the DBTT derived from the Charpy impact data to monitor irradiation embrittlement was originally used for RPV ferritic steels. It is therefore interesting to compare the mechanical properties of a martensitic steel (Eurofer-97) to those of a ferritic steel (18MND5, a typical reactor pressure vessel steel with 0.18C, 0.25Si, 1.55Mn, 0.008P, 0.002S, 0.18Cr, 0.13Cu, 0.50Mo, 0.64Ni wt%) with a tempered bainitic microstructure. The grain size is also different, ~9 μm for Eurofer-97 and ~22 μm for 18MND5. The 18MND5 experimental data were taken from [60]. Fig. 9 shows the Charpy impact energy transition curves of both steels. The ductile-to-brittle transition curve of 18MND5 is much smoother than Eurofer-97. In addition, the upper shelf energy level of 18MND5 is significantly lower than Eurofer-97. Similar trends are shown by the transition curves based on the shear fracture appearance (Fig. 10) and lateral expansion. Based on classical transition temperature parameters, Figs. 9 and 10 are suggesting better toughness properties of the Eurofer-97 than of the 18MND5. Moreover, the tearing resistance of Eurofer-97 is higher than for 18MND5.

As already indicated, the shape of the Charpy impact transition curve varies from one material to another. The shape of the curve is believed to stem from the micromechanical processes acting during fracture of the Charpy specimen. Indeed, it is known that, from the observation of a fracture surface, many processes coexist during the fracture of a Charpy specimen [26]. In the transition regime,

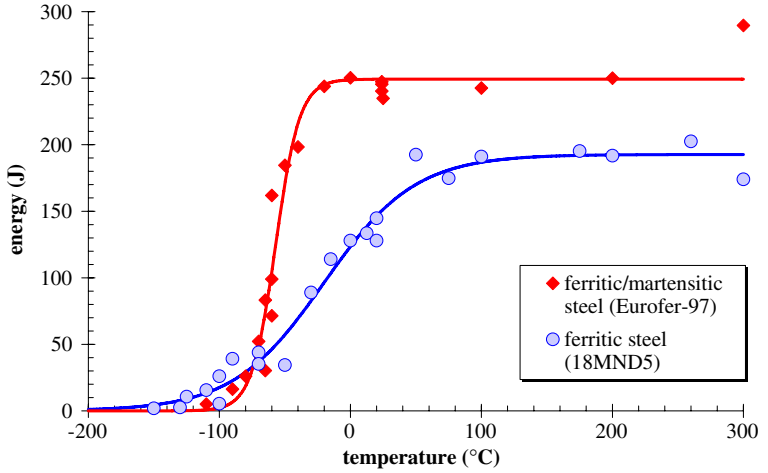

Fig. 9. Charpy impact energy transition curve: Eurofer-97 versus 18MND5.

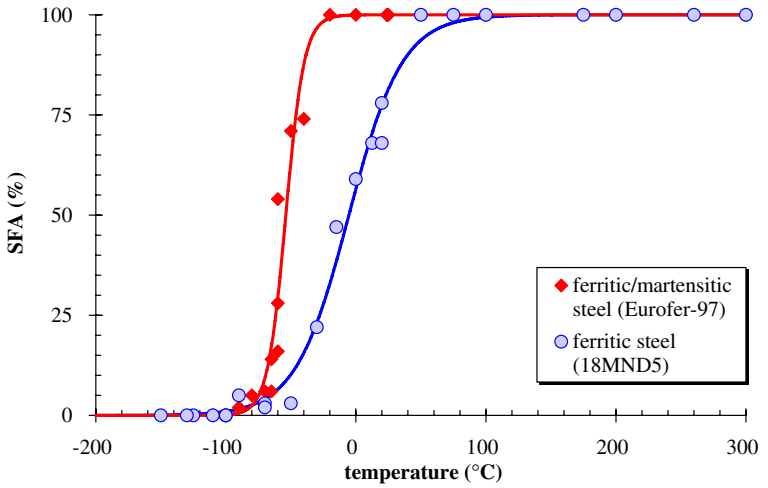

Fig. 10. Charpy impact SFA transition curve: Eurofer-97 versus 18MND5.

this includes successively ductile crack initiation, stable crack growth, unstable (brittle) fracture, crack arrest and finally shear lips formation [26]. Of course, the relative contribution of each individual process varies with the test temperature. For instance, in the lower shelf, at sufficiently low temperature, no ductile crack growth is observed while at the upper shelf, only ductile cracking occurs. The load diagram can help identifying the various contributions. These diagrams for both Eurofer-97 and 18MND5 materials are compared in Fig. 11. The characteristic parameters are summarized in Table 4. As it can be seen, these two steels present many similarities but also some differences that are described in the following.

The temperature T_I of both steels is very similar suggesting similar condition for brittle fracture. The fracture toughness transition temperatures of both steels are also very similar (see Fig. 12), in accordance with Fig. 6. The microcleavage fracture stress of Eurofer-97 is higher than of 18MND5 indicating a better resistance to cleavage initiation. The strain rate sensitivity of Eurofer-97 is higher than of 18MND5. The temperature range of the transition region is shorter for Eurofer-97 than for 18MND5. In particular, the onset of the ductile upper shelf occurs at a lower temperature for Eurofer-97 in comparison to 18MND5. Similarly, the crack arrest properties of Eurofer-97 are superior to those of 18MND5. It is known that grain

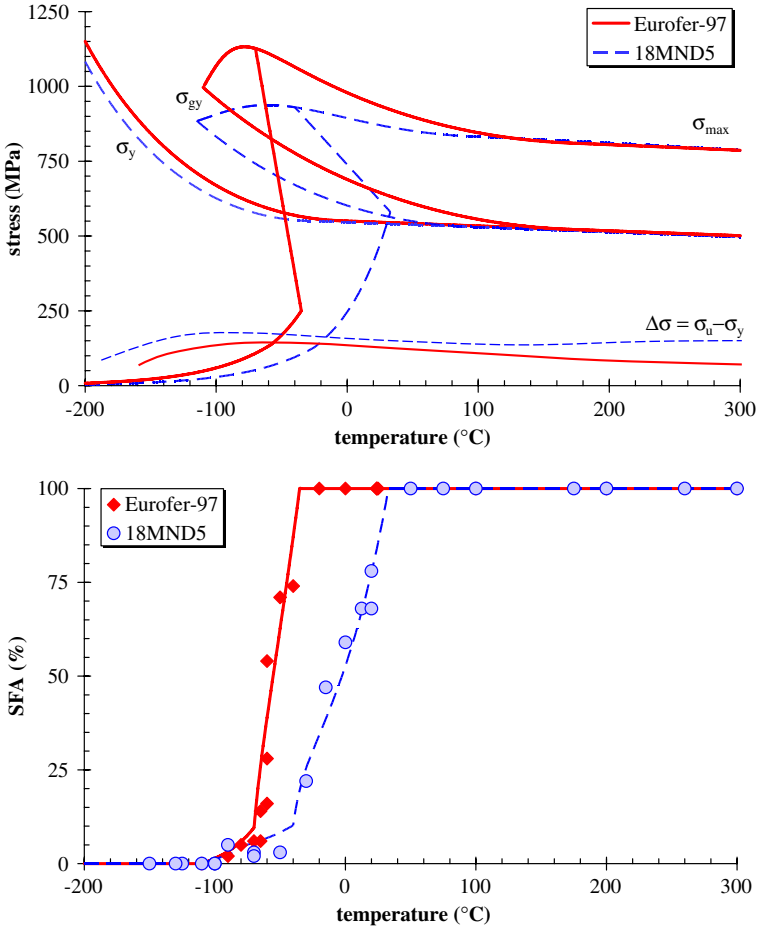

Fig. 11. Load diagram of Eurofer-97 in comparison to 18MND5 and their associated SFA-diagram.

Table 4
Characteristic parameters of Eurofer-97 versus 18MND5

Material	σ_{ath} (MPa)	σ_c (MPa)	T_I (°C)	T_O (°C)	T_{NDT} (°C)	FATT (°C)	$T_{100\,MPa\sqrt{m}}$ (°C)	$J_{0.2\,dyn}$ (kJ/m^2)	$J_{t\,dyn}$ (kJ/m$^2\sqrt{mm}$)
Eurofer-97	595	2342	−110	−35	−58	−56	−115	428	841
18MND5	590	2081	−115	33	−25	−3	−119	372	637

boundaries offer an important resistance to cleavage crack resistance. This is related to the high angle grain boundary misorientation of the martensitic microstructure which improves the crack arrest performance of cleavage microcracks [61–63]. Unfortunately, no detailed microstructural examination was performed to better relate the microstructure to the mechanical properties.

As expected from the upper shelf energy levels, Eurofer-97 has a better tearing resistance than 18MND5. This is confirmed by the crack resistance curves shown in Fig. 13. These are the main differences when comparing Eurofer-97 to 18MND5 and this is illustrated in Fig. 14. After the maximum load, for Eurofer-97, a small increase of the test temperature promotes ductile fracture rather than cleavage. This has to be associated with a better cleavage resistance of Eurofer-97. The flow properties being comparable, cleavage initiation is more easily reached in 18MND5. Indeed, because of the higher microcleavage strength of Eurofer-97, a small increase of temperature significantly reduces the probability of cleavage fracture. This explains also the shape of the transition curve of Eurofer-97 that is steeper

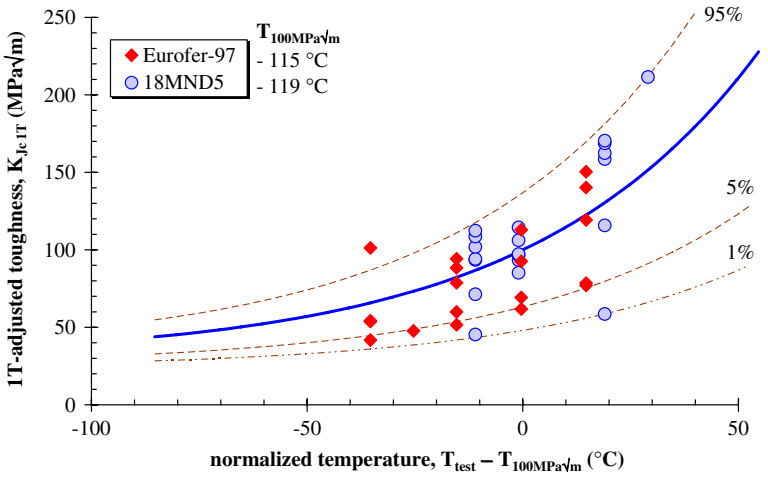

Fig. 12. Fracture toughness in the transition regime: Eurofer-97 versus 18MND5.

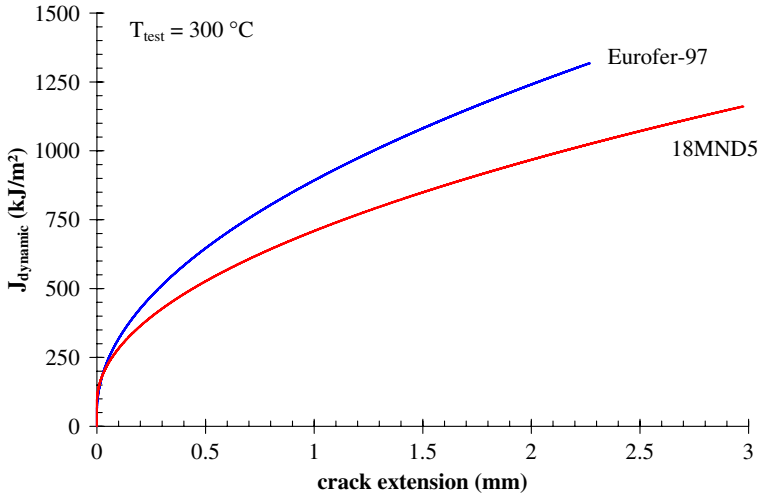

Fig. 13. Crack resistance behavior at 300 °C at dynamic loading rate: Eurofer-97 versus 18MND5.

than for 18MND5. The steepness of the transition curve over a narrow temperature range can be evaluated through the difference $T_O - T_I$, which is 75 °C and 148 °C for Eurofer-97 and 18MND5, respectively. A steep transition curve is also characteristic of a clean microstructure, Eurofer-97 containing less second phase particles than 18MND5. As a result, the probability of finding a microstructural defect under stress–strain conditions favorable for cleavage initiation is higher in 18MND5. The comparison between Eurofer-97 and 18MND5 in terms of fracture toughness transition temperature and crack resistance parameters were also indicated in Table 4. The transition temperatures T_I and $T_{100\,MPa\sqrt{m}}$ are in very good agreement. The differences between T_O, T_{NDT} and other classical transition temperatures (based on energy, SFA and lateral expansion) are reflected by the differences between both the cleavage and ductile crack resistance performances of Eurofer-97 and 18MND5.

Lucas et al. [54] have raised the question on the shape of the transition curve and the underlying role of microstructure. It is clear that the shape of the transition curve is related to the microstructure of the material and to the competition between cleavage and ductile fracture. Grain size, density and size of the particles (inclusions, carbides) and other precipitation hardening and impurity segregation play a role in the way fracture occurs in the transition regime. Unfortunately, the materials

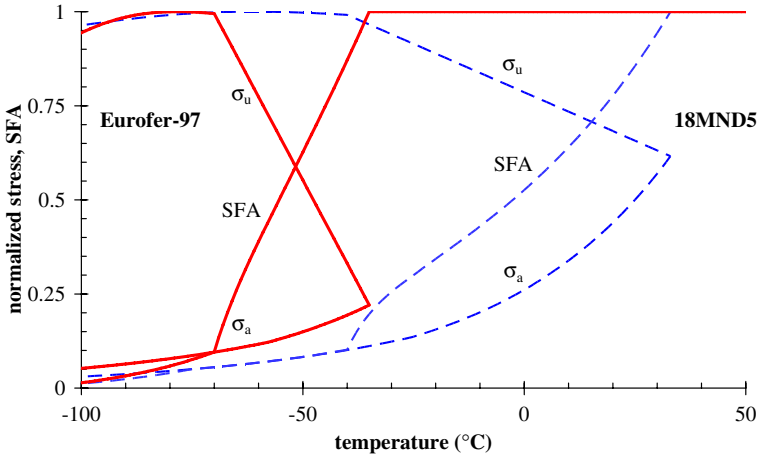

Fig. 14. Main differences between Eurofer-97 and 18MND5 in the transition region.

investigated here were not examined from the microstructural point of view. Nevertheless, some information found in literature for Eurofer-97 [16,17] indicates a microstructure consisting of laths of tempered martensite of about 0.5 μm wide, MnS-inclusions, Ta-rich inclusions and few more other inclusion types with their size respectively in the range of 1.2–1.7 μm, 1.2–1.7 μm and ~4 μm. Cr-rich precipitates, $M_{23}C_6$-type, finely dispersed along lath interfaces and prior austenite grain boundaries and sometimes inside subgrains were identified, with their size ranging between 0.06 and 0.3 μm, 0.05 and 0.2 μm, 0.5 μm, respectively. For the 18MND5, MnS inclusions are typical for these materials and the carbides are mainly Mo_2C-type. Also M_3C cementite precipitates can be found. Although quantitative measurements on 18MND5 are missing, the size of the inclusions is usually higher than the particles found in Eurofer-97 (from few μm to few tens of μm).

At T_I, the fracture is typically cleavage, resulting from an unstable propagation of a microcrack initiated at a brittle trigger particle. The high local stress/strain conditions prevailing at the crack tip process zone induce microcracks at inclusions and carbides. Most of microcracks will arrest into the adjacent matrix material and the microcracks eligible for propagation are those with sufficient large size favorably oriented to induce a macroscopic cleavage fracture. The matrix material is tempered martensite and tempered bainite for Eurofer-97 and 18MND5, respectively. Based on the material parameters shown in Table 4, in particular the microcleavage fracture stress, Eurofer-97 requires higher local stresses, or equivalently a higher fracture surface energy, to induce cleavage. This can be microstructurally associated with the size and density of particles present in the material [64]. Examination of the load diagrams shown in Fig. 11 suggests that the particle density and distribution in Eurofer-97 is more uniform and homogeneous than in 18MND5. This means that in Eurofer-97, the temperature range over which cleavage fracture may occur after stable crack extension is narrow. By contrast, in 18MND5, because of the heterogeneous particle distribution, this temperature range of cleavage fracture preceded with ductile crack extension is larger. This is also consistent with the superior crack arrest and crack resistance properties of Eurofer-97 in comparison to 18MND5. It is believed that the nature, size and distribution density of the particles present in Eurofer-97 provide a good compromise between a good strength and a good crack resistance to both cleavage and ductile fracture. It is the combination of fine precipitate dispersion of carbide particles in a tough tempered martensite that provides Eurofer-97 with such good properties. On the other hand, an eligible particle for cleavage initiation after ductile extension can easily be found in 18MND5.

In conclusion, to explain the difference between the transition curves of Eurofer-97 and 18MND5, two main factors can be put forward:

1. Eurofer-97 (with a tempered martensite microstructure) has a better resistance to both brittle and ductile cracking than 18MND5 (with a tempered bainite microstructure);

2. the abrupt transition curve of Eurofer-97 in comparison to 18MND5 can be related to the size, density and distribution of the second phase particles present in the materials (inclusions, carbides). It is believed that a much finer and uniform distribution of particles is present in Eurofer-97 than in 18MND5.

It is interesting to examine also the tensile properties of Eurofer-97 and 18MND5 as in literature these are often correlated with the fracture resistance behavior. The tensile curves of Eurofer-97 and 18MND5 are shown in Fig. 15. As it can be seen, the yield and ultimate tensile strengths of both steels are comparable, only elongations and work hardening are different. Examination of Table 4 and Fig. 15 clearly shows that the elements that are usually put forward to improve fracture toughness, namely, a high work hardening capacity and high uniform and total elongations, do not systematically lead to an improved fracture resistance. Despite a lower work hardening capacity and lower elongations, Eurofer-97 exhibits a significantly better crack resistance than 18MND5. This is not specific to the materials examined here but was also observed on other materials and test conditions [53].

The Charpy impact transition curve is also used to estimate the material tearing resistance. Indeed, the upper shelf energy level is assumed to be proportional to the tearing resistance, the higher the upper shelf energy, the higher the ductile initiation toughness and tearing resistance of the material. However, this is true as far as the same fracture mechanisms are concerned and ignoring possible loading rate effects. For example, in Fig. 1, the upper shelf energy is little affected by irradiation. However, crack resistance measurements performed on statically loaded precracked three-point bend specimens indicated a drastic decrease of initiation toughness and tearing resistance (see Fig. 16) [65]. This drastic degradation of the tearing properties result from a change of the fracture mechanism (presence of plastic flow localization) associated with loading rate effects. This phenomenon, out of the scope of the present paper, is reported elsewhere [65].

7. Discussion

Examination of the results presented in the previous sections clearly emphasizes the importance of combining the various mechanical properties to better understand the material behavior. Conclusions on irradiation effects solely based on tensile tests or DBTT measurements should be considered with caution. Only a global approach integrating a number of mechanical (flow and fracture) properties can provide a reliable assessment of the material degradation.

In the following, this global approach will be illustrated on a typical example of Eurofer-97 irradiated at 300 °C up to 1.55 dpa. The load diagrams in both the unirradiated and irradiated conditions are shown in Fig. 17. The increase of the athermal part of the yield strength results in an increase of the transition temperatures T_I, T_{NDT}, T_O and $T_{50\%}$. The shift of T_I measures the brittle transition temperature increase and can be compared to the

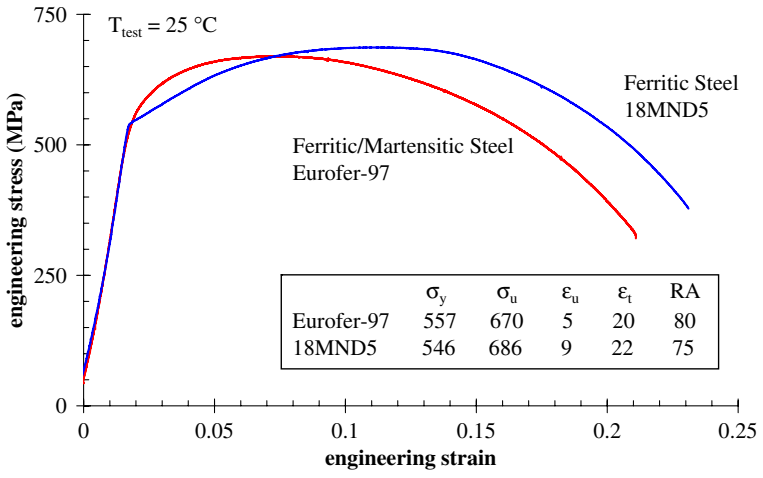

Fig. 15. Engineering stress–strain flow behavior: Eurofer-97 versus 18MND5.

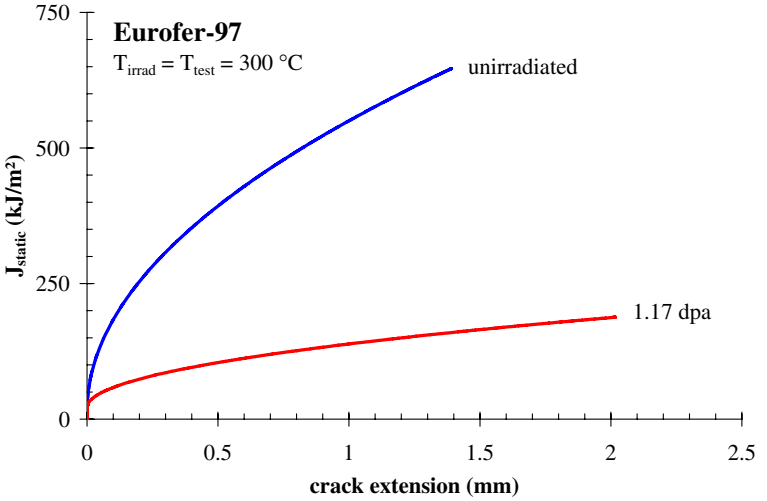

Fig. 16. Effect of irradiation on the crack resistance behavior of Eurofer-97.

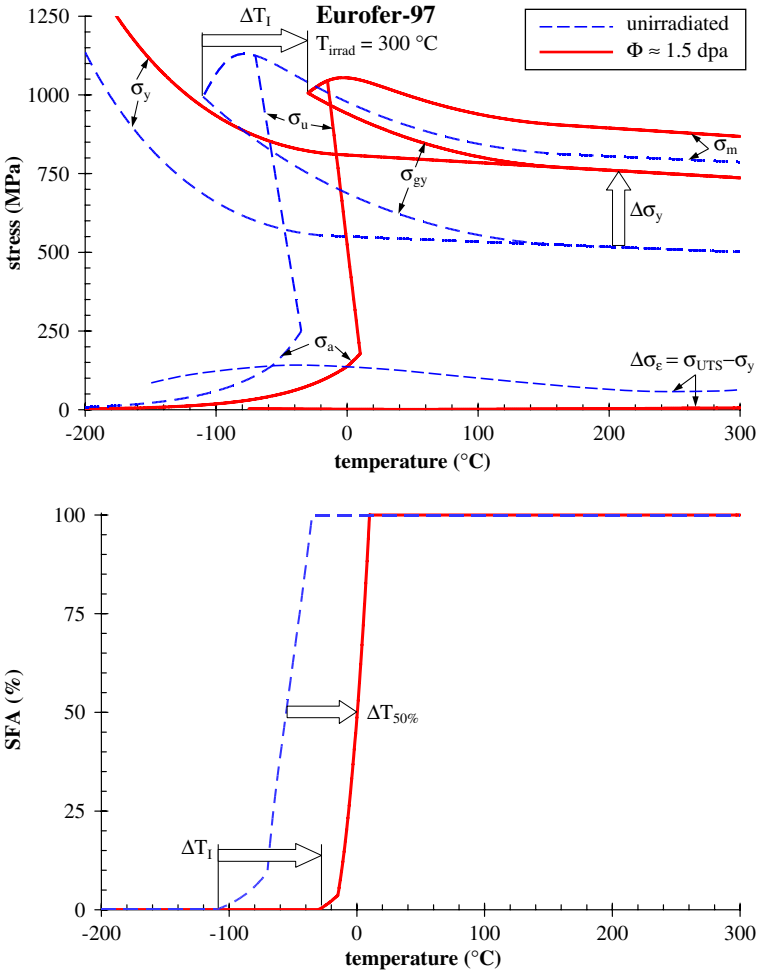

Fig. 17. Effect of irradiation on the load diagram of Eurofer-97.

shift of the fracture toughness transition curve, $\Delta T_{100\,\mathrm{MPa}\sqrt{\mathrm{m}}}$. The lack of work hardening capacity measured by $\Delta\sigma_\varepsilon = \sigma_{\mathrm{UTS}} - \sigma_{\mathrm{y}}$ where σ_{UTS} and σ_{y} are the ultimate tensile and yield strength, respectively, of the irradiated material indicates its susceptibility for plastic flow localization. The latter is not necessarily reflected by the Charpy impact data as measured by the difference between the maximum stress, σ_{m}, and the general yield stress, σ_{gy}, namely, $\Delta\sigma = \sigma_{\mathrm{m}} - \sigma_{\mathrm{gy}}$. Indeed, the static upper shelf toughness can be much more affected than what the upper shelf energy might suggests. A change of ductile fracture mechanism is suspected to occur when loading rate is changed [66].

The mechanisms of brittle (cleavage) fracture initiation in ferritic/martensitic steels are not so different from those operating in ferritic steels. As a result, the master curve procedure can be applied to characterize fracture toughness in the transition regime. However, the shape of the master curve could be different in the upper transition region. Indeed, in the unirradiated condition, the load diagram analysis and the ductile crack resistance measurements indicate a possible abrupt increase of fracture toughness in the upper transition regime. Experimental measurements using large specimens would be very helpful to examine if the fracture toughness transition curve shape can be represented by the master curve. On the other hand, for the irradiated condition, because of the irradiation-induced plastic flow localization, the fracture mechanism is affected and may influence the shape of the master curve. Further investigations are required to verify if the shape of the master curve is changed or not.

Contrary to initially designed, the Charpy impact test is not anymore used as a screening test to evaluate effects related to material chemistry, heat treatment, environmental effects. Nowadays, it is involved in the definition of the appropriate material that can be used in extreme operating conditions. An illustration on the possible misinterpretation of the use of Charpy impact data is given by the very known figure due to Kohyama et al. [67] showing the effect of chromium content on the DBTT-shift of ferritic/martensitic steels (see also [68]). This figure indicates a minimum DBTT-shift around 9%Cr-content and therefore is often used, among other interesting properties, to justify the choice of 9%Cr-steels in irradiation environments [38,68]. It is likely that the actual DBTT-shift is little affected by Cr-content and the observed DBTT-shift is biased by the DBTT determination procedure. The effect of increasing Cr-content modifies the microstructure of the steel from a ferrite (bainitic) one to a tempered martensite around 9%Cr. Above 10%Cr, the microstructure is not a fully tempered martensite but contains some δ-ferrite as well. In ferritic steels, the DBTT is evaluated at a much lower energy level, usually 41 J for RPV steels. This explains why ferritic steels do show a good correlation between the Charpy-based DBTT-shift and the fracture toughness based transition temperature shift but not for the tempered martensitic steels. The 9%-Cr steels with respect to low-Cr steels have certainly a number of interesting properties such as corrosion, creep and swelling resistance but not for irradiation embrittlement.

Investigations directed towards the effect of chemical composition, tempering heat treatment and irradiation should not be based solely on the DBTT alone. Other parameters including the tensile properties and detailed Charpy impact data analyses are required to unambiguously characterize the materials. Anomalies such as those reported in literature on the inconsistency between DBTT-change, upper shelf energy change and yield strength increase [25,58,59,69–72] can be clarified if examined in a consistent approach combining all available properties. Finally, it is important to mention the large interest of using miniature specimen test techniques, in particular the small punch test [73,74]. The small punch test data are usually correlated to Charpy impact data to assess fracture in the transition regime. Careful examination of these tests should be carried out before reliable information on the effects of irradiation can be extracted.

8. Conclusions

There is a long tradition in the scientific community to monitor irradiation effects on mechanical properties of structural materials by examining the shift of the DBTT measured using Charpy impact data. It is shown in this paper that depending on the definition of the DBTT, the conclusions that might be drawn can be very misleading. Combining all available properties in a consistent manner, such as the load diagram, can be very helpful in better understanding the material properties and also provides a quality control tool of the experimental results. Alternatively, the level at which the DBTT is evaluated should be decreased to a level where fracture is typically brittle. Another parameter derived from the Charpy impact data is the upper

shelf energy that usually correlates well with the material resistance to ductile crack extension. It is also found here that this is not always the case. In particular, in presence of plastic flow localization, the upper shelf energy largely underestimates the decrease of ductile initiation toughness and tearing resistance.

This work has clarified the importance of using physically based rather than empirical parameters to monitor irradiation effects on the mechanical response of ferritic/martensitic steels.

Acknowledgements

The author gratefully acknowledges the support of M. Decréton, E. Lucon, A. Pellettieri, J.L. Puzzolante, L. Van Houdt and P. Wouters. Thanks to D. Maes for reviewing the paper.

References

[1] A.L. Hiser, in: F.A. Garner et al. (Eds.), Influence of Radiation on Material Properties: 13th International Symposium, Part II, ASTM STP 956, ASTM, 1987, p. 333.
[2] F.J. Schmitt, in: N.H. Packan et al. (Eds.), Effect of Radiation on Materials: 14th International Symposium, vol. II, ASTM STP 1046, ASTM, 1990, p. 373.
[3] K. Onizawa, M. Suzuki, in: S.T. Rosinski et al. (Eds.), Effect of Radiation on Materials: 20th International Symposium, ASTM STP 1405, ASTM, 2001, p. 79.
[4] I.J. O'Donnell, R. Combie, Int. J. Press. Vess. Piping 67 (1996) 299.
[5] A. Fabry, J. Van de Velde, J.L. Puzzolante, T. Van Ransbeeck, A. Verstrepen, E.C. Biemiller, R.G. Carter, T. Petrova, in: D.S. Gelles et al. (Eds.), Effects of Radiation on Materials: 17th International Symposium, ASTM STP 1270, ASTM, 1996, p. 138.
[6] G.R. Odette, G.E. Lucas, J. Nucl. Mater. 117 (1983) 276.
[7] E 1921, Standard test method for determination of reference temperature, T_0, for ferritic steels in the transition range, Annual Book of ASTM Standards, Section 3, Metals Test Methods and Analytical Procedures, vol. 03.01, American Society for Testing and Materials, 2002.
[8] E. Lucon, J. Nucl. Mater. 329–333 (2004) 1078.
[9] J. Rensman, J. van Hoepen, J.B.M. Bakker, R. den Boef, F.P. van den Broek, E.D.L. van Essen, J. Nucl. Mater. 307–311 (2002) 245.
[10] J. Rensman, H.E. Hofmans, E.W. Schuring, J. van Hoepen, J.B.M. Bakker, R. den Boef, F.P. van den Broek, E.D.L. van Essen, J. Nucl. Mater. 307–311 (2002) 250.
[11] E. Lucon, Characterization of the mechanical properties of EUROFER in the unirradiated and irradiated condition, SCK·CEN report BLG-945, 2003.
[12] E. Lucon, Mechanical properties of the European reference RAFM steel (EUROFER-97) before and after irradiation at 300 °C (0.3–2 dpa), SCK·CEN report BLG-962, 2003.
[13] R.L. Klueh, D.R. Harries, High-Chromium Ferritic and Martensitic Steels for Nuclear Applications, ASTM, 2001.
[14] R. Andreani, E. Diegele, R. Laesser, B. van der Schaaf, J. Nucl. Mater. 329–333 (2004) 20.
[15] J. Rensman, E. Lucon, J. Boskeljon, J.V. Hoepen, R. Den Boef, P. Ten Pierick, J. Nucl. Mater. 329–333 (2004) 1113.
[16] P. Fernandez, A.M. Lancha, J. Lapena, M. Hernandez-Mayoral, Fus. Eng. Des. 58–59 (2001) 787.
[17] P. Fernandez, A.M. Lancha, J. Lapena, M. Serrano, M. Hernandez-Mayoral, J. Nucl. Mater. 307–311 (2002) 495.
[18] P. Fernandez, M. Garcia-Mazario, A.M. Lancha, J. Lapena, J. Nucl. Mater. 329–333 (2004) 273.
[19] R. Lindau, M. Schirra, Fus. Eng. Des. 58–59 (2001) 781.
[20] R. Lindau, A. Möslang, M. Schirra, Fus. Eng. Des. 61&62 (2002) 659.
[21] P. Spätig, G.R. Odette, G.E. Lucas, M. Victoria, J. Nucl. Mater. 307–311 (2002) 536.
[22] E. Daum, K. Ehrlich, M. Schirra, in: Proceedings of the 2nd Milestone Meeting of European Laboratories, Kalsruhe, FZKA-5848, 1997.
[23] D.J. Alexander, R.L. Klueh, in: J.M. Holt (Ed.), Charpy Impact Test; Factors and Variables, ASTM STP 1072, ASTM, 1990, p. 179.
[24] M.A. Sokolov, R.K. Nanstad, in: D.S. Gelles et al. (Eds.), Effects of Radiation on Materials: 17th International Symposium, ASTM STP 1270, ASTM, 1996, p. 384.
[25] E. Lucon, A. Almazouzi, Mechanical response to irradiation for three high-Cr martensitic steels (EM10, T91, HT9) – Intermediate Report: 1st Specimen Batch (2.6 dpa), SCK·CEN report BLG-973, 2004.
[26] R. Chaouadi, A. Fabry, in: D. François, A. Pineau (Eds.), From Charpy to Present Impact Testing, Elsevier Science and ESIS, 2002, p. 103.
[27] A. Fabry, E. van Walle, R. Chaouadi, J.P. Wannijn, A. Verstrepen, J.L. Puzzolante, T. Van Ransbeeck, J. Van de Velde, T. Petrova, RPV steel embrittlement – Damage modeling and micromechanics in an engineering perspective, SCK·CEN report BLG-649, 1993.
[28] A. Fabry, Nuclear reactor pressure vessel integrity insurance by crack arrestability evaluation using loads from instrumented CVN tests, SCK·CEN report BLG-750, 1997.
[29] A.S. Tetelman, A.J. McEvily, Fracture of Structural Materials, John Wiley, 1967.
[30] R.L. Klueh, N. Nashimoto, M.A. Sokolov, J. ASTM Int. 1 (2004).
[31] H.C. Schneider, B. Dafferner, J. Aktaa, J. Nucl. Mater. 321 (2003) 135.
[32] R.L. Klueh, M.A. Sokolov, K. Shiba, Y. Miwa, J.P. Robertson, J. Nucl. Mater. 283–287 (2000) 478.
[33] R.L. Klueh, D.J. Alexander, in: R.K. Nanstad et al. (Eds.), Effects of Radiation on Materials: 18th International Symposium, ASTM STP 1325, ASTM, 1999, p. 911.
[34] R.L. Klueh, D.J. Alexander, J. Nucl. Mater. 265 (1999) 262.
[35] R.L. Klueh, D.J. Alexander, M.A. Sokolov, J. Nucl. Mater. 304 (2002) 139.
[36] M. Rieth, B. Dafferner, H.D. Rödig, J. Nucl. Mater. 258–263 (1998) 1147.
[37] I. Belianov, P. Marny, J. Nucl. Mater. 258–263 (1998) 1259.
[38] R.L. Klueh, D.J. Alexander, J. Nucl. Mater. 233–237 (1996) 336.
[39] L. Schäfer, M. Schirra, K. Ehrlich, J. Nucl. Mater. 233–237 (1996) 264.
[40] P. Gondi, R. Montarani, A. Sili, M.E. Tata, J. Nucl. Mater. 233–237 (1996) 248.

[41] J.C. Brachet, A. Castaing, C. Foucher, Proceedings of an International Symposium on Materials Ageing and Component Life Extension, vol. 1, Engineering Materials Advisory Services, 1995, p. 75.
[42] M. Rieth, B. Daffener, H.D. Röhrig, C. Wassilew, Fus. Eng. Des. 29 (1995) 365.
[43] R.L. Klueh, D.J. Alexander, J. Nucl. Mater. 212–215 (1994) 736.
[44] J.L. Séran, V. Lévy, P. Dubuisson, D. Gilbon, A. Maillard, A. Fissilo, H. Touron, R. Cauvin, A. Chalony, E. Le Boulbin, in: R.E. Stoller et al. (Eds.), Effects of Radiation on Materials: 15th International Symposium, ASTM STP 1125, ASTM, 1992, p. 1209.
[45] R.L. Klueh, D.J. Alexander, P.J. Maziasz, J. Nucl. Mater. 186 (1992) 185.
[46] R.L. Klueh, D.J. Alexander, J. Nucl. Mater. 179–181 (1991) 733.
[47] L. Schäfer, in: C. Varandas, F. Serra (Eds.), Fusion Technology, Elsevier Science, 1997, p. 1367.
[48] R.L. Klueh, P.J. Maziasz, in: N.H. Packan et al. (Eds.), Effects of Radiation on Materials, vol. I, ASTM STP 1046, ASTM, 1989, p. 246.
[49] R.L. Klueh, J.M. Vitek, W.R. Corwin, D.J. Alexander, J. Nucl. Mater. 155–157 (1988) 973.
[50] W.R. Corwin, R.L. Klueh, J.M. Vitek, J. Nucl. Mater. 122–123 (1984) 343.
[51] B.S. Louden, A.S. Kumar, F.A. Garner, M.L. Hamilton, J. Nucl. Mater. 155–157 (1988) 662.
[52] M. Victoria, D. Gavillet, P. Spätig, F. Rezai-Aria, S. Rossmann, J. Nucl. Mater. 233–237 (1996) 326.
[53] R. Chaouadi, Flow and fracture behavior of 9%Cr–ferritic/martensitic steels, SCK·CEN report R-4122, 2005.
[54] G.E. Lucas, G.R. Odette, K. Edsinger, B. Wirth, J.W. Sheckherd, in: D.S. Gelles et al. (Eds.), Effects of Radiation on Materials: 17th International Symposium, ASTM STP 1270, ASTM, 1996, p. 790.
[55] M. Rieth, B. Dafferner, J. Nucl. Mater. 233–237 (1996) 229.
[56] K. Edsinger, G.R. Odette, G.E. Lucas, J.W. Sheckherd, J. Nucl. Mater. 233–237 (1996) 342.
[57] I. Belianov, P. Marmy, J. Nucl. Mater. 258–263 (1998) 1259.
[58] W.L. Hu, D.S. Gelles, in: F.A. Garner et al. (Eds.), Influence of Radiation on Material Properties: 13th International Symposium, Part II, ASTM STP 956, ASTM, 1987, p. 83.
[59] J. Rensman, E.V. van Osch, M.G. Horsten, D.S. d'Hulst, J. Nucl. Mater. 283–287 (2000) 1201.
[60] R. Chaouadi, M. Scibetta, E. Lucon, A. Fabry, J.L. Puzzolante, E. van Walle, Test results and evaluation of radiation-induced shifts of the transition behavior of two PWR vessel steels: 18MND5 and JRQ, SCK·CEN report R-3340, 1999.
[61] Y. Qiao, A.S. Argon, Mech. Mater. 35 (2003) 313.
[62] E. Bouyne, P. Joly, B. Houssin, C. Wiesner, A. Pineau, Fat. Fract. Eng. Mater. Struct. 24 (2001) 105.
[63] A.F. Gougues, H.M. Flower, T.C. Lindley, Mater. Sci. Technol. 16 (2000) 26.
[64] G.E. Lucas, H. Yih, G.R. Odette, J. Nucl. Mater. 155–157 (1988) 673.
[65] R. Chaouadi, Assessment of the effects of neutron irradiation on the mechanical properties of Eurofer-97 ferritic/martensitic steel, SCK·CEN report R-4257, 2005.
[66] R. Chaouadi, Effect of irradiation-induced plastic flow localization on ductile crack resistance behavior of a 9%Cr tempered martensitic steel, submitted for publication.
[67] A. Kohyama, A. Hishinuma, D.S. Gelles, R.L. Klueh, W. Dietz, K. Ehrlich, J. Nucl. Mater. 233–237 (1996) 138.
[68] A. Hishinuma, A. Kohyama, R.L. Klueh, D.S. Gelles, W. Dietz, K. Ehrlich, J. Nucl. Mater. 258–263 (1998) 193.
[69] M. Suzuki, K. Fuyaka, T. Kodaira, T. Oku, in: F.A. Garner et al. (Eds.), Influence of Radiation on Material Properties: 13th International Symposium, Part II, ASTM STP 956, ASTM, 1987, p. 98.
[70] M.L. Hamilton, L.E. Schubert, D.S. Gelles, in: F.A. Garner, A.S. Kumar (Eds.), Effects of Radiation on Materials: 18th International Symposium, ASTM STP 1325, ASTM, 1999, p. 931.
[71] Y. Dai, P. Marmy, J. Nucl. Mater. 343 (2005) 247.
[72] N.S. Cannon, D.S. Gelles, J. Nucl. Mater. 186 (1991) 68.
[73] Y. Dai, X.J. Jia, K. Farrell, J. Nucl. Mater. 318 (2003) 192.
[74] X.J. Jia, Y. Dai, J. Nucl. Mater. 323 (2003) 360.